Journal of Hydrology 661 (2025) 133673

Contents lists available at ScienceDirect

Journal of Hydrology

journal homepage: www.elsevier.com/locate/jhydrol

Research papers

Divergent drought-induced suppression on vegetation and associated feedbacks: Satellite-based observations in 2022 across the Yangtze River basin, China

Lei Han[a,b], Yanan Chen[b], Chaoyang Wu[c], Li Yao[d,*], Ying Wang[b], Chao Su[a], Xuan Li[a], Alexandre Maniçoba da Rosa Ferraz Jardim[e], Thieres George Freire da Silva[f], Xuguang Tang[a,*]

[a] Institute of Remote Sensing and Geosciences, Hangzhou Normal University, Hangzhou 311121, China
[b] School of Geographical Sciences, Southwest University, Chongqing 400715, China
[c] Key Laboratory of Land Surface Pattern and Simulation, Institute of Geographical Sciences and Natural Resources Research, Chinese Academy of Sciences, Beijing 100101, China
[d] School of Culture and Tourism, Zhejiang International Studies University, Hangzhou 310023, China
[e] Department of Biodiversity, Institute of Biosciences, São Paulo State University UNESP, Av. 24A, 1515, Rio Claro, São Paulo 13506-900, Brazil
[f] Department of Plant Production, Academic Unit of Serra Talhada, Federal Rural University of Pernambuco, Gregório Ferraz Nogueira Avenue, SN, Serra Talhada 56909-535 Pernambuco, Brazil

A R T I C L E I N F O

This manuscript was handled by Marco Borga, Editor-in-Chief, with the assistance of Hanbo Yang, Associate Editor

Keywords:
Drought effects
Vegetation indices
Resistance and resilience
Vulnerability
Yangtze River basin

A B S T R A C T

During the summer of 2022, a record-breaking drought event coupled with unprecedentedly low rainfall struck in the Yangtze River basin (YRB) of China. However, the quantitative assessment of the consequences of such extreme drought event remains a significant challenge, which hinders the development of effective mitigation strategies and the enhancement of ecosystem resilience. This study synthesized three satellite remote sensing-based vegetation indices to evaluate the potential effects of such extreme drought, including the solar-induced chlorophyll fluorescence (GOSIF), normalized difference vegetation index (NDVI) and near-infrared reflectance of vegetation (NIR_V). Furthermore, a novel 'resistance–resilience' framework was proposed to explore the mechanisms underlying vegetation responses to extreme drought. The results revealed that regions surrounding the Sichuan Basin, Guizhou Plateau, and Jiangnan Hills were the most severely affected area. Moreover, the summer drought of 2022 led to a marked reduction in vegetation growth across most vegetated areas, as evidenced by negative detrended anomalies in GOSIF (73.7 %), NDVI (90.9 %) and NIR_V (80.9 %). Among different vegetation types, evergreen broadleaf forests suffered the most significant reduction, whereas a slight increase happened in grasslands. Furthermore, an inverse relationship was revealed between vegetation resistance and resilience, characterized by weak resistance-strong resilience or strong resistance-weak resilience. Specifically, grasslands in high altitudes exhibited higher resistance with lower resilience, while forests in the Sichuan Basin and Jiangnan Hills generally showed lower resistance with higher resilience. Evergreen broadleaf forests, in particular, are expected to face heightened vulnerability owing to the impact of future droughts. All analyses provide a critical framework for evaluating the potential effects of drought extremes on plant structures and functions, and offers valuable insights for land managers to support sustainable management practices.

1. Introduction

In recent decades, global climate change has profoundly impacted the structure and function of terrestrial ecosystems, attracting serious concerns from nations and societies worldwide. With the progression of global warming, extreme climate events have become more frequent on the global scale. Among the main abiotic stresses affecting terrestrial ecosystems, droughts caused significant damages to both human society and natural ecosystems (Piao et al., 2019; AghaKouchak et al., 2020). For instance, the severe drought in 2003 led to tens of thousands of deaths, widespread forest wildfires, and a reduction in gross primary productivity (GPP) in Europe by approximately 30 %, resulting in a

* Corresponding authors.
E-mail addresses: yao66625@zisu.edu.cn (L. Yao), xgtang@swu.edu.cn (X. Tang).

https://doi.org/10.1016/j.jhydrol.2025.133673
Received 7 March 2025; Received in revised form 27 May 2025; Accepted 6 June 2025
Available online 7 June 2025

significant release of carbon into the atmosphere (Wang et al., 2023a; García-Herrera et al., 2010; Ciais et al., 2005). Furthermore, satellite remote sensing detected a significant decline in vegetation greenness and productivity, severely disrupting the regional carbon cycle during the 2022 summer drought in the Yangtze River basin of China (Wang et al., 2023a; Xu et al., 2024). Several studies have indicated that since July 2022, the ongoing La Niña event has contributed to the expansion and intensification of the western Pacific subtropical high-pressure system, leading to unprecedented extreme drought events in many regions globally (Li et al., 2024; Sun et al., 2022; Wang et al., 2023a). Therefore, a deep understanding of vegetation dynamics in response to drought is crucial for assessing the vulnerability of terrestrial ecosystems, which offers theoretical support for the realization of national carbon neutral strategies (Jiang et al., 2024; Liu et al., 2023a).

Satellite-based remote sensing provides an effective means for the continuous observation of vegetation changes from regional to global levels. Various vegetation indices (VIs), such as solar-induced chlorophyll fluorescence (SIF), normalized differential vegetation indice (NDVI) and near-infrared reflectance of vegetation (NIR_V), are used to detect the drought-induced anomalies in vegetation dynamics (Li et al., 2024; Wang et al., 2023a). Among these, SIF has been proven to effectively track global vegetation productivity and has the advantages of capturing vegetation's physiological states. Since SIF is emitted from the chlorophyll of actively photosynthesizing plants, it is less impacted by snow cover compared to other indices (Li et al., 2023; Meng et al., 2021). As a proxy of vegetation greenness, NDVI provides valuable insights into vegetation photosynthetic activity and stress monitoring. Nevertheless, the VI is susceptible to soil conditions, being readily influenced by soil composition and water content. Moreover, NDVI often reaches its limit in assessing multi-layered, dense vegetation, limiting its effectiveness in such complicated environment (Huang et al., 2021c; Pettorelli et al., 2005). The recently-developed NIR_V index not only addresses the issue of mixed pixel, but also can effectively capture vegetation photosynthesis (Badgley et al., 2017). By integrating the effects of leaf area, leaf orientation, and overall canopy structure, NIR_V has been demonstrated in several studies to serve as an effective proxy for monitoring the effect of drought on terrestrial ecosystems across different spatial scales (Qiu et al., 2022; Chen et al., 2025).

Recent studies have introduced a 'Resistance–Resilience' framework to quantify ecosystem function responses to climate extremes across various biomes (Nimmo et al., 2015; Yao et al., 2024; Isbell et al., 2015; Huang and Xia, 2019). This framework is grounded in the general concept that ecological units, such as ecosystems, communities, populations, and individuals, respond to disturbances through a process involving both resistance during the event and recovery afterward (Nimmo et al., 2015). Vegetation resistance is defined as the ability of ecosystem to maintain its structure and function during disturbances, thereby quantifying the direct impact of these disturbances on ecosystem functioning (Bellanthudawa and Chang, 2022; Cole et al., 2014). The resilience of vegetation is defined as an ecosystem's capacity to return to its undisturbed condition and functioning after experiencing a disturbance (Ingrisch and Bahn, 2018). Vegetation vulnerability is affected not only by its vegetation resistance to such drought event but also by its ability to recover quickly afterward (Vicente-Serrano et al., 2010). Hence, evaluating vegetation vulnerability requires considering both its resistance and recovery capacities (Jiang et al., 2024). Within this framework, plenty of studies have highlighted the variations in drought resistance and resilience of vegetation across different scales (Gazol et al., 2018; Cole et al., 2014; De Keersmaecker et al., 2015; Liu et al., 2023a; Han et al., 2024). However, direct quantification of regional ecosystem resistance and resilience to droughts by measuring changes in ecosystem functioning during and after droughts remains rare (Huang and Xia, 2019). Given the increasing frequency of extreme drought events projected for the future, the resistance and resilience of global biomes are anticipated to decline to varying degrees (Liu et al., 2023a). Consequently, investigating the vegetation resistance, resilience and vulnerability to drought events across different areas is crucial for accurately quantifying vegetation responses (Chen et al., 2018).

The Yangtze River basin (YRB) is a critical ecological barrier in China, playing a crucial role in maintaining ecological balance and security at both regional and national levels. Its unique geographical location, pronounced sea-land temperature gradients, and seasonal alterations in atmospheric circulation make this area particularly susceptible and vulnerable to the disturbances of changing climate (Chen et al., 2020). In the summer of 2022, extreme drought events in the YRB exposed approximately 360 million people in China to temperatures exceeding 40 °C. In addition to the extreme heat wave, the region experienced severe drought and widespread wildfires, leading to socioeconomic losses totaling $7.6 billion (Xu et al., 2024; Chen et al., 2024; Li et al., 2024). Then, Xing et al. (2024) comprehensively analyzed the drought characteristics by comparing historical typical years with 2022 drought in the YRB.

Previous studies have employed traditional vegetation indices to assess potential drought-induced impacts (Liu et al., 2023a; Zeng et al., 2022), while significant research gaps persist in quantitatively evaluating vegetation response mechanisms to drought-induced stress. Therefore, in order to strengthen our understanding of the 2022 summer drought and associated vegetation responses, we integrated three satellite-based ecological indicators including the NDVI, NIR_V and SIF, along with the Standardized Precipitation and Evaporation Index (SPEI) dataset and proposed a new 'resistance-resilience' framework: (1) to reveal the spatio-temporal evolution processes of drought in the summer of 2022 across the Yangtze River basin; (2) to explore the potential impact of such drought event on terrestrial vegetation dynamics; and (3) to assess ecosystem resistance, resilience and vulnerability to the extreme drought event across various biomes. These analyses are expected to deepen our understanding of the impacts of drought extremes on the structures and functions of vegetation as well as the associated feedbacks.

2. Materials and methods

2.1. Description of the study area

The YRB extends from the eastern part of the Qinghai-Tibet Plateau to the East China Sea, spanning the western, central, and eastern economic regions of China (Fig. 1). This area is one of the most economically powerful and strategically significant regions in China. Additionally, the YRB serves as a crucial ecological barrier, playing a critical role in protecting ecological balance and security at both regional and national levels (Huang et al., 2023). However, climate extremes have become increasingly frequent in the region. As a result, the basin has become more sensitive and vulnerable to climate change, particularly to severe droughts, which undoubtedly pose a threat to food production, vegetation growth and water resources supply (Chen et al., 2020). Consequently, it represents an optimal region for examining the response of drought events across various eco-geographical zones and vegetation types (Li et al., 2024).

In our study, the YRB was divided into eight eco-geographical zones based on temperature and moisture conditions. These divisions were defined as the Qinghai-Tibet Plateau (HIB1/C1), Western Sichuan-Eastern Tibet Plateau (HIIA/B1), Guizhou Plateau (VA3), Sichuan Basin (VA4), Yunnan Plateau (VA5), Middle and Lower Yangtze River Basin (IVA1), Hanzhong Basin (IVA2), and Jiangnan Hills (VA1/VA2) (Fig. 1b, Table S1). Among them, we define the zones of HIB1/C1, HIIA/B1 and VA5 as high-altitude regions. Detailed information regarding these divisions can be found on the website of the Resource and Environment Science and Data Center, Chinese Academy of Sciences (https://www.resdc.cn/data.aspx?DATAID=125). The major vegetation types are derived from MODIS land cover data (MCD12C1 v061), which is available at https://lpdaac.usgs.gov/products/mcd12c1v061/. This study focused on the vegetated areas in the YRB, with barren land and

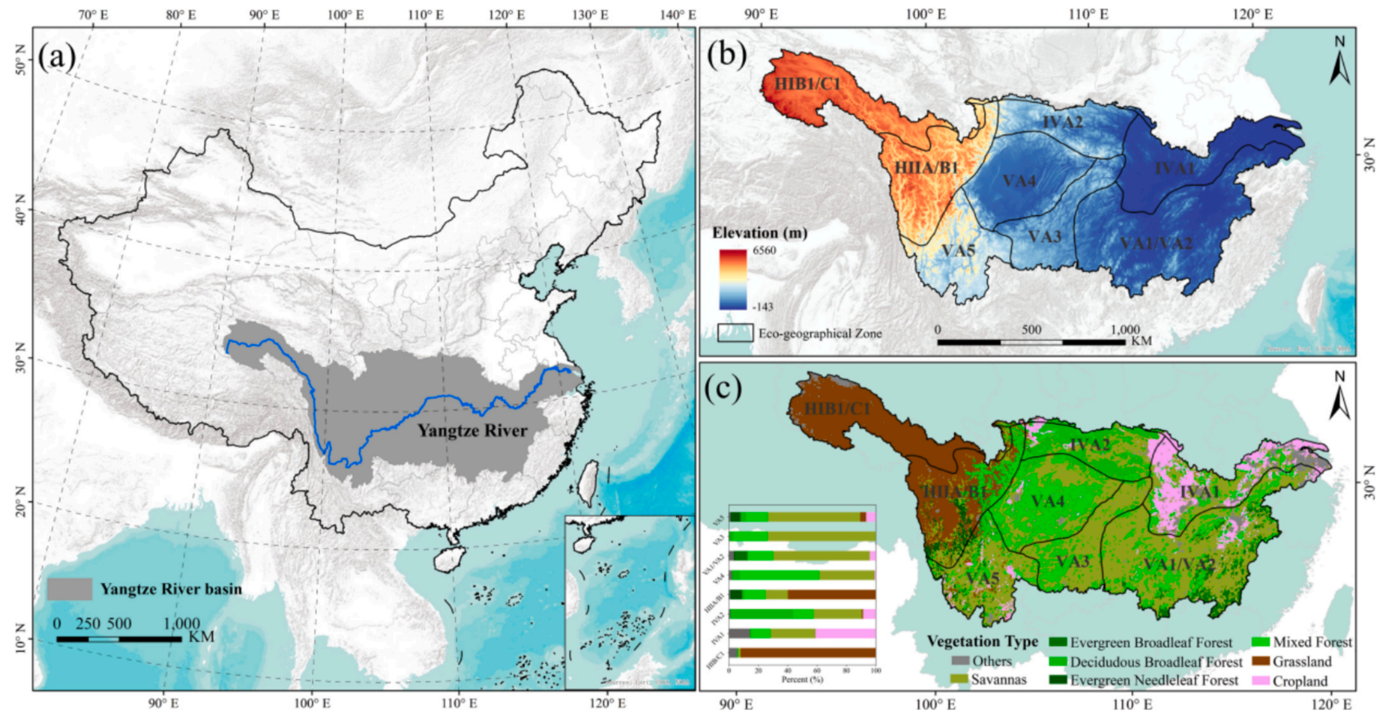

Fig. 1. Spatial pattern of the Yangtze River basin (YRB) in China, including (a) geographic location and distribution of main stream, (b) the digital elevation data and its eight eco-geographical zones, and (c) the main vegetation types. The inserted bar chart in Fig. 1(c) showed the percentage distribution of vegetation types across the eight eco-geographical regions.

ice areas masked and excluded from the analysis. The evergreen broadleaf forest (EBF), evergreen needleleaf forest (ENF), mixed forest (MF), deciduous broadleaf forest (DBF), savanna (SA), cropland (CRO) and grassland (GRA) were extracted as major natural vegetation types referring to the International Geosphere Biosphere Program (IGBP), with a spatial resolution of 0.05° (Fig. 1c).

2.2. Multi-source satellite remote sensing data

The study utilized multiple satellite-based remote sensing datasets, including solar-induced chlorophyll fluorescence (SIF) data, MODIS-NDVI data, MODIS-NIR_V data, the European Centre for Medium-Range Weather Forecasts (ECMWF) Reanalysis over land data (ERA5-Land, V5). Specific attribute information for each dataset is provided in Table S2. With an 8-day temporal scale, discrete OCO-2 SIF retrievals, the Moderate Resolution Imaging Spectroradiometer (MODIS) data, and meteorological reanalysis data were used to support the Cubist regression tree model that was used to create the GOSIF dataset (Li and Xiao, 2019). It was accessible from 2000 to 2023 through the Global Ecology Group of the University of New Hampshire (website: http://data.globalecology.unh.edu/data/GOSIF_v2/). The integrated SIF-GPP relationship produced 8-day GPP estimates showing high consistency ($R^2 = 0.74$, RMSE = 1.92 W m^{-2} μm^{-1} sr^{-1}) with eddy covariance measurements from 91 global FLUXNET sites. Therefore, GOSIF is a perfect tool for evaluating vegetation photosynthesis and ecosystem status. Plant photosynthetic activity can now be directly characterized globally due to the GOSIF dataset's better geographical resolution, continuous global coverage, and comprehensive temporal records (Li et al., 2023a).

The Global Monthly NDVI and near-infrared (NIR) datasets were derived from the MODIS-based MOD13C2 products. The NDVI dataset was generated by the Ecological Forecasting Lab of the NASA Ames Research Center (Ding et al., 2022). The average reflectance values of high-quality 1-km pixels are aggregated to 0.05° to create the Climate Modeling Grid (CMG, 0.05° resolution) VI product. A quality assurance filter scheme is then applied to remove lower-quality, cloud-contaminated pixels (Huete et al., 2010). This study utilized the QA band of MOD13C2 for preliminary data screening, retaining pixels with `VI Quality' flags of 0 (Good data) and 1 (Marginal data). For missing values in the time series, a reconstruction method combining Savitzky-Golay filtering with local spatial interpolation was applied (Chen et al., 2004). Near-infrared reflectance of terrestrial vegetation (NIR_V) is a recently-proposed vegetation index that reflects the canopy structure and photosynthetic ability to a certain extent (Badgley et al., 2017). NIR_V is favored over conventional vegetation indices because it can distinguish the signal from vegetation, address the challenges of mixed pixels, and partially alleviate the impacts of background luminosity and soil interference (Zhang et al., 2022). We calculated the NIR_V by combining the MODIS NDVI and NIR, as described by Badgley et al. (2017):

$$NIR_V = (NDVI - 0.08) \times NIR \tag{1}$$

To maintain consistency in spatial resolution with SIF, the time series of NDVI and NIR_V datasets were selected for the period from 2003 to 2023, encompassing a total of 252 months.

ERA5 is the latest global climate reanalysis dataset, provided by the European Centre for Medium-Range Weather Forecasts (ECMWF) through the Copernicus Climate Change Service (C3S). The ERA5 reanalysis dataset combines numerical weather prediction models and historical observation data to offer high-resolution information on various atmospheric, land, and ocean surface variables globally from 1979 to the present (Muñoz-Sabater et al., 2021). We used the monthly 0.1° climate data, encompassing the air temperature at 2 m and precipitation, for the period from 2003 to 2022.

Finally, the satellite-based GOSIF, NDVI, and NIR_V data were detrended using the linear regression method as described by Bai et al. (2020). This detrending method can effectively eliminate the linear trend in annual time series while preserving seasonal variations and ensures that the detrended data for the first year remains consistent with the original data.

2.3. Methods

2.3.1. Characteristics of drought event

There are various indicators for monitoring drought, among which the commonly used meteorological drought indices include the Standardized Precipitation Index (SPI), Palmer Drought Severity Index (PDSI). However, recent studies have revealed certain limitations in these indices. For instance, the PDSI involves computationally complex procedures and lacks multi-timescale characterization (Ding et al., 2020). While the SPI demonstrates multi-timescale adaptability, it solely considers precipitation while neglecting evapotranspiration and temperature variations (Naresh Kumar et al., 2009). The Standardized Precipitation Evapotranspiration Index (SPEI) is a regional meteorological drought monitoring indicator established by Vicente-Serrano et al. (2021), building upon the Standardized Precipitation Index (SPI). It quantifies drought severity by measuring the deviation between the potential evapotranspiration and precipitation from the average state. The SPEI covers periods ranging from 1 to 48 months, reflecting the aggregate water status (either scarcity or abundance) from the prior timeframe. As a result, this data enables the identification and characterization of various drought events (Wang et al., 2021a). In our study, we calculated potential evapotranspiration (PET) on a monthly scale using temperature dataset from ERA5 by Thornthwaite (1948). Then based on the monthly precipitation and PET dataset, we employed the "gma" package in Python to calculate the three-month SPEI ($SPEI_3$) for detecting extreme drought in the YRB during summer 2022, given its effectiveness in tracking short-term fluctuations in soil moisture conditions (Xu et al., 2015). Additionally, droughts were classified into five levels based on associated SPEI thresholds proposed by Xu et al. (2015) as follows (see Table 1):

2.3.2. Resistance and resilience of vegetation to droughts

Severe climate events, like heatwaves and droughts, posed serious risks to terrestrial ecosystems as well as society (Han et al., 2024; Tang et al., 2017). Recent studies have introduced an ecosystem stability framework (resistance and resilience), offering a novel approach to assessing ecosystem function responses to extreme climates across diverse biotic communities (Nimmo et al., 2015; De Keersmaecker et al., 2014; Li et al., 2020b), as depicted in Fig. 2. Examining vegetation responses to drought from the perspective of resistance and resilience can enhance efforts to prevent and manage vegetation degradation, providing theoretical guidance for national carbon neutrality strategic decision-making.

Vegetation resistance to drought events is characterized by the inverse relationship between relative annual monthly vegetation dynamics during such events. Besides, the variance in relative monthly vegetation dynamics anomalies between periods during and after drought events is used to evaluate the resilience of vegetation (Isbell et al., 2015; Jiang et al., 2024). Evaluating vegetation resistance and resilience requires the calculation of Standardized Anomalies (SA) for monthly Vegetation Indices (VIs) including SIF, NDVI and NIR_V. The SA for monthly VIs (SA_{VIs}) was calculated at each pixel as below (Wang et al., 2021a):

$$SA_{VIs} = \frac{VIs_{i,t} - \overline{VIs_{i,t}}}{\delta(VIs_{i,t})}\ (t = 1, 2, \cdots, 12) \tag{2}$$

Table 1
Five drought types defined by SPEI threshold values.

Levels	Types	SPEI
1	No drought	$-0.5 < SPEI$
2	Mild drought	$-1.0 < SPEI \leq -0.5$
3	Moderate drought	$-1.5 < SPEI \leq -1.0$
4	Severe drought	$-2.0 < SPEI \leq -1.5$
5	Extreme drought	$SPEI \leq -2.0$

where $VIs_{i,t}$ is the value of VIs at the *i* grid for the *t* month during the drought event, $\overline{VIs_{i,t}}$ is the mean value of VIs at the *i* grid for the *t* month from 2003 to 2023, and $\delta(VIs_{i,t})$ is standard deviation (SD) of VIs at *i* grid for the *t* month over the reference period.

Considering the disparity between the normalized deviations preceding the drought and those occurring during the event, vegetation resistance was modified based on the state of the vegetation previous to the drought. The period of vegetation resilience was delineated as the interval commencing with the onset of a drought and extending to the month when the impact on vegetation peaks. Vegetation recovery time refers to the period between the month of maximum impact and the month of optimal recovery. The best month for recovery is when there is a positive standardized anomaly in VIs after a drought event ends and a subsequent decline in the month that follows (Fig. 2). The definitions of vegetation resistance and resistance time are showed as below (Isbell et al., 2015; Jiang et al., 2024):

$$\text{Resistance} = \frac{1}{G_e^{Anomaly} - G_0^{Anomaly}} \tag{3}$$

$$G_0^{Anomaly} = \frac{G_t^{Anomaly} + G_{t-1}^{Anomaly}}{2} \tag{4}$$

$$\text{Resistance time} = t_i - t_0 \tag{5}$$

where $G_e^{Anomaly}$ denotes the anomaly in VIs on the most severe drought month, while $G_0^{Anomaly}$ refers to the anomaly in VIs before the drought. $G_t^{Anomaly}$ is the anomaly in VIs that occurs at the start of the drought, and $G_{t-1}^{Anomaly}$ refers to the anomaly in VIs that occurs in the month preceding the start of the drought.

The capacity of vegetation to recover can be quantified through the application of the subsequent formulas (Isbell et al., 2015; Jiang et al., 2024):

$$\text{Resilience} = \left|G_e^{Anomaly} - G_r^{Anomaly}\right| \tag{6}$$

$$\text{Recovery time} = t_r - t_i \tag{7}$$

where $G_r^{Anomaly}$ stands for the standardized anomaly of VIs in the best recovery month.

Resistance and resilience are dimensionless quantities that allow for comparisons between diverse ecosystems and disturbance kinds. Vegetation exhibiting higher resistance and resilience scores showcases a stronger capacity to endure and bounce back from drought conditions (Isbell et al., 2015; Jiang et al., 2024). In our study, two sets of vegetation resistance and resilience are calculated by using GOSIF, MODIS NDVI and NIR_V datasets, and then averaged.

2.3.3. Vulnerability of vegetation to droughts

Vulnerability is often defined in terms of exposure, sensitivity, and resilience. However, recent attempts to quantify this impact have primarily focused on measuring exposure to climate change, largely ignoring the resistance and resilience of ecosystems, which can significantly influence vulnerability assessments (Li et al., 2018). According to the IPCC, resistance and recovery capabilities of the impacted processes should be considered when evaluating vegetation vulnerability (Mitchell et al., 2016; Smith et al., 2014). The framework for integrated ecosystem resistance and resilience presents a novel method for studying vegetation vulnerability quantitatively. Thus, both vegetation resistance and resilience were taken into account when evaluating the vegetation vulnerability to drought events. The subsequent equation illustrates that the susceptibility of vegetation is in direct opposition to its resistance and resilience:

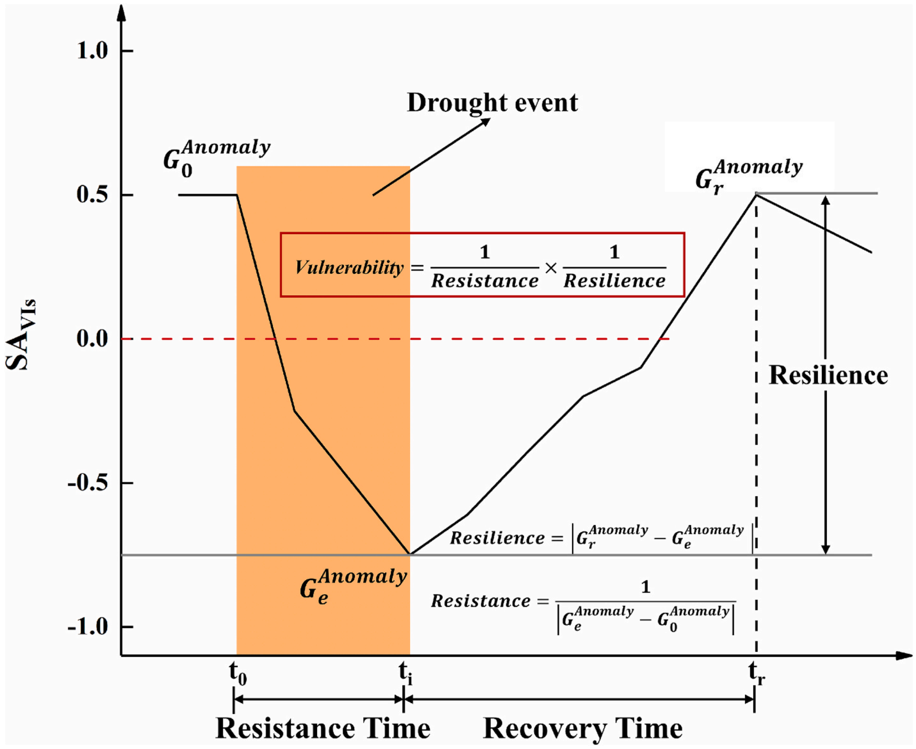

Fig. 2. Schematic diagram of vegetation resistance and resilience during the drought event.

$$\text{Vulnerability} = \frac{1}{\text{Resistance}} \times \frac{1}{\text{Resilience}} = \frac{\left|G_e^{\text{Anomaly}} - G_0^{\text{Anomaly}}\right|}{\left|G_e^{\text{Anomaly}} - G_r^{\text{Anomaly}}\right|} \tag{8}$$

where G_e^{Anomaly} represents the anomaly in VIs during the most severe drought month, while G_0^{Anomaly} represents the anomaly in VIs prior to the drought. G_r^{Anomaly} represents the standardized anomaly of VIs in the best recovery month.

In this study, the ecosystem stability metrics used (resistance, resilience, and vulnerability) are all dimensionless indices. Therefore, they can be directly applied to compare ecosystems with different productivity levels without being restricted by units. Additionally, these indices exhibit symmetry and can be used to compare the impacts of different disturbance events. It should be noted that a higher resistance indicates less reduction in vegetation during external disturbances, but this does not necessarily imply a longer resistance time. Stronger resilience suggests that the vegetation can recover to the optimal original state after a

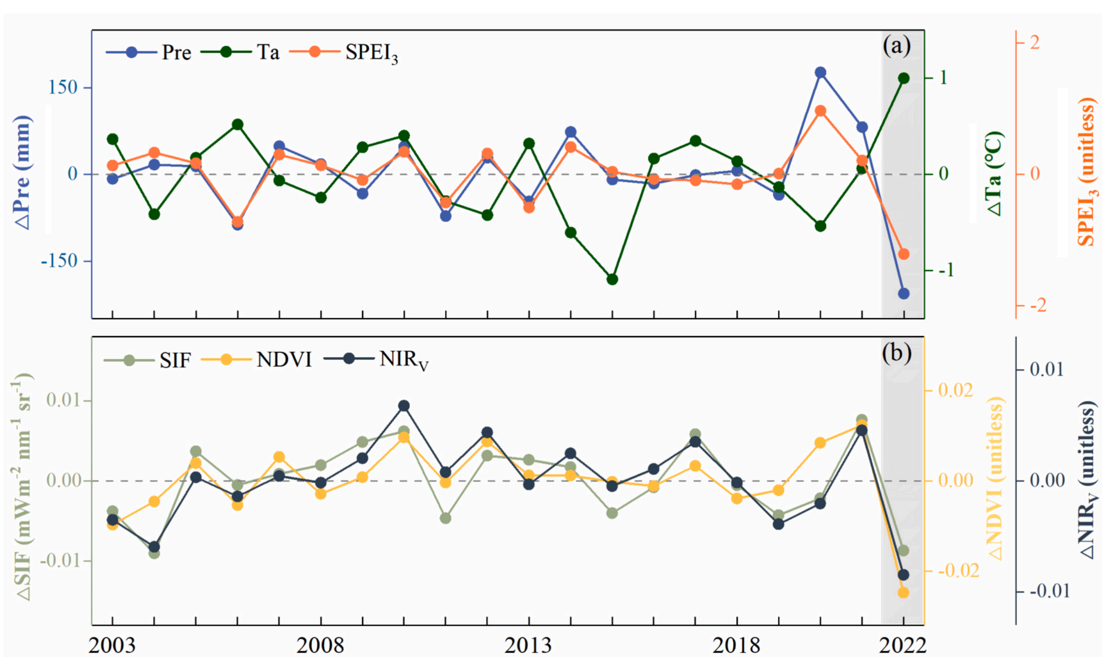

Fig. 3. Anomalies in the detrended temperature (ΔTa), precipitation (ΔPre), $SPEI_3$, SIF (ΔSIF), NDVI (ΔNDVI) and NIR_V (ΔNIR_V) during summer (July–September) from 2003 to 2022 in the Yangtze River basin, China.

drought, but vegetation with stronger resilience may also have a longer recovery time. In order to provides a holistic view of ecosystem stability, we calculated a set of vegetation vulnerability metrics for the YRB based on SIF, NDVI, and NIR_V, and then averaged. Lastly, we analyzed the magnitudes of vegetation vulnerability across different vegetation types in the YRB.

3. Results

3.1. Evolution processes of the 2022 summer drought

Climatic variables (air temperature and precipitation) and the drought index ($SPEI_3$) broke records for the 2003–2022 period in the summer of 2022 (Fig. 3a). The sustained influence of an exceptionally strong Western Pacific Subtropical High triggered a prolonged, large-scale, and high-impact heatwave over the YRB, leading to the high-temperature (+1.0 °C) and low-precipitation (–206.3 mm) anomaly during summer 2022 (Fig. 3a). According to the $SPEI_3$ anomaly (–1.2), the summer of 2022 was the hottest and driest since meteorological data began in China. It is well established that extreme temperatures and dry air can have a significant impact on terrestrial ecosystems. Vegetation response to drought is evident not only in structure changes but also in its physiological processes. In our study, this drought event resulted in the most severe anomalies in SIF (–0.01), NDVI (–0.02) and the NIR_V (–0.01) since 2003 (Fig. 3b).

As shown in Fig. 4, this study illustrated spatio-temporal dynamics of the summer 2022 drought in the YRB based on $SPEI_3$. In July 2022, 63.1 % of the YRB experienced drought conditions, primarily in the form of moderate drought (23.8 %). In August 2022, both the extent and severity of the drought intensified, with 85.5 % of the YRB affected, predominantly characterized as severe drought (34.4 %). Till September 2022, nearly the entire YRB was experiencing drought conditions, with 35.1 % under extreme drought, 46.2 % under severe drought, 14.5 % under moderate drought, and 3.4 % under mild drought. The most severely affected regions included the Western Sichuan-Eastern Tibet Plateau, the Sichuan Basin, the Guizhou Plateau, the middle and lower Yangtze River basin, and the Jiangnan Hills. Overall, approximately 89 % of the YRB experienced severe drought conditions during the summer of 2022, with particularly intense impacts observed in subregions including IVA1, IVA2, and VA4.

3.2. Effects of the 2022 summer drought on vegetation

As shown in Fig. 5, the extreme drought event significantly suppressed the growth of vegetation during the summer of 2022, as reflected by the negative detrended anomalies in three vegetation indices. Spatially, the majority of the vegetated regions showed negative detrended anomalies for GOSIF (73.7 %), NDVI (90.9 %), and NIR_V (80.9 %) during the summer. In August 2022, the proportion of grids with negative anomalies for NDVI and NIR_V reached its peak, accounting for 92.1 % and 80.7 %, respectively, while the proportion of negative anomalies for GOSIF reached its highest in September 2022 at 77.3 %. Additionally, we analyzed the spatial uniformity of detrended anomalies across three different vegetation indices. Our findings indicated that during the summer of 2022, the spatial consistency of detrended anomalies for these three indices was preserved across 67.9 % of the grid cells, and 65.1 % of the grids show negative detrended anomalies, while 2.8 % of the grids display positive anomalies (Fig. 5m). Negative anomalies were primarily concentrated in the VA4, VA3, IVA2 and IVA1, while positive anomalies were mainly mostly observed in parts of the HIIA/B1 and VA5. Furthermore, the NDVI and NIR_V values decreased to their lowest recorded levels during the period of summer 2022 (as depicted in Supplementary Fig. S1b,c). Similar to the record low in 2004, the detrended anomalies for GOSIF in the summer of 2022 reached the second-lowest level ever documented (Fig. S1a). Notably, the drop across three vegetation indicators peaked in September 2022, even though GOSIF increased slightly in July 2022 (Fig. S1j-l).

The timing of the most extensive vegetation stress, as indicated by the three vegetation indices, varied during extreme drought events. We determined that the periods with the lowest detrended vegetation index anomalies corresponded to times of maximum vegetation stress. The lowest detrended anomaly in SIF occurred in September (Fig. 6a), and the response of NDVI followed a similar pattern (Fig. 6b and Figs. S2 and S3 in Supplementary Material). In contrast, NIR_V exhibited an earlier onset of vegetation stress compared to SIF and NDVI, with the lowest anomaly recorded in August (Fig. 6c). In addition, the recovery times of

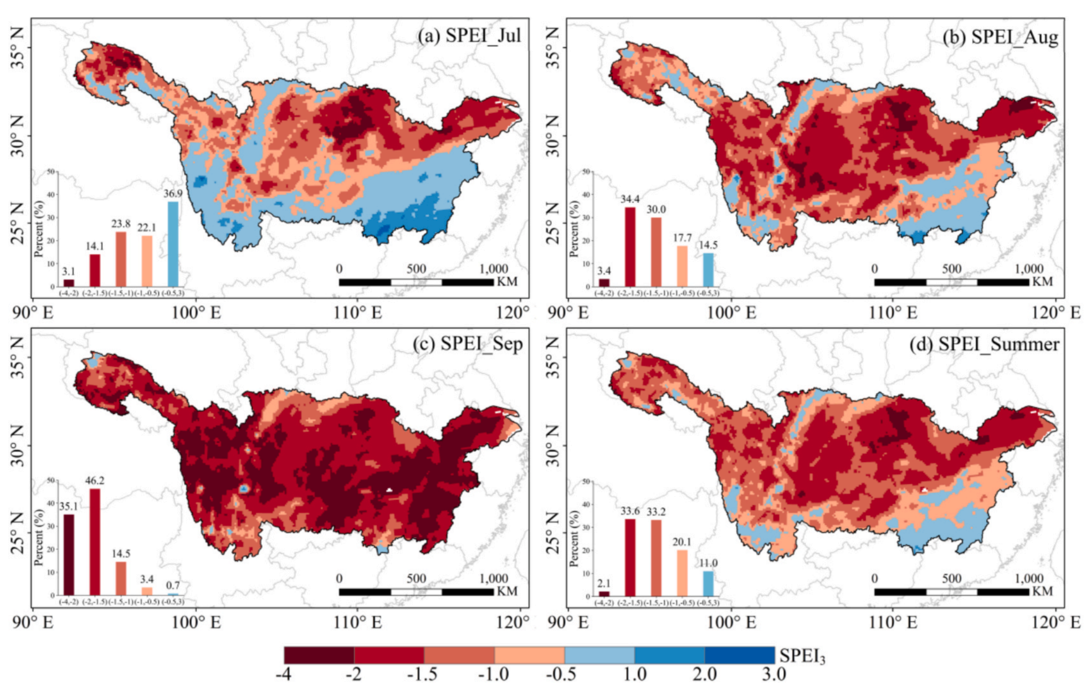

Fig. 4. Spatio-temporal dynamics of the 2022 summer drought in the Yangtze River basin based on $SPEI_3$, with the bar chart as a proxy for the proportions of different drought levels.

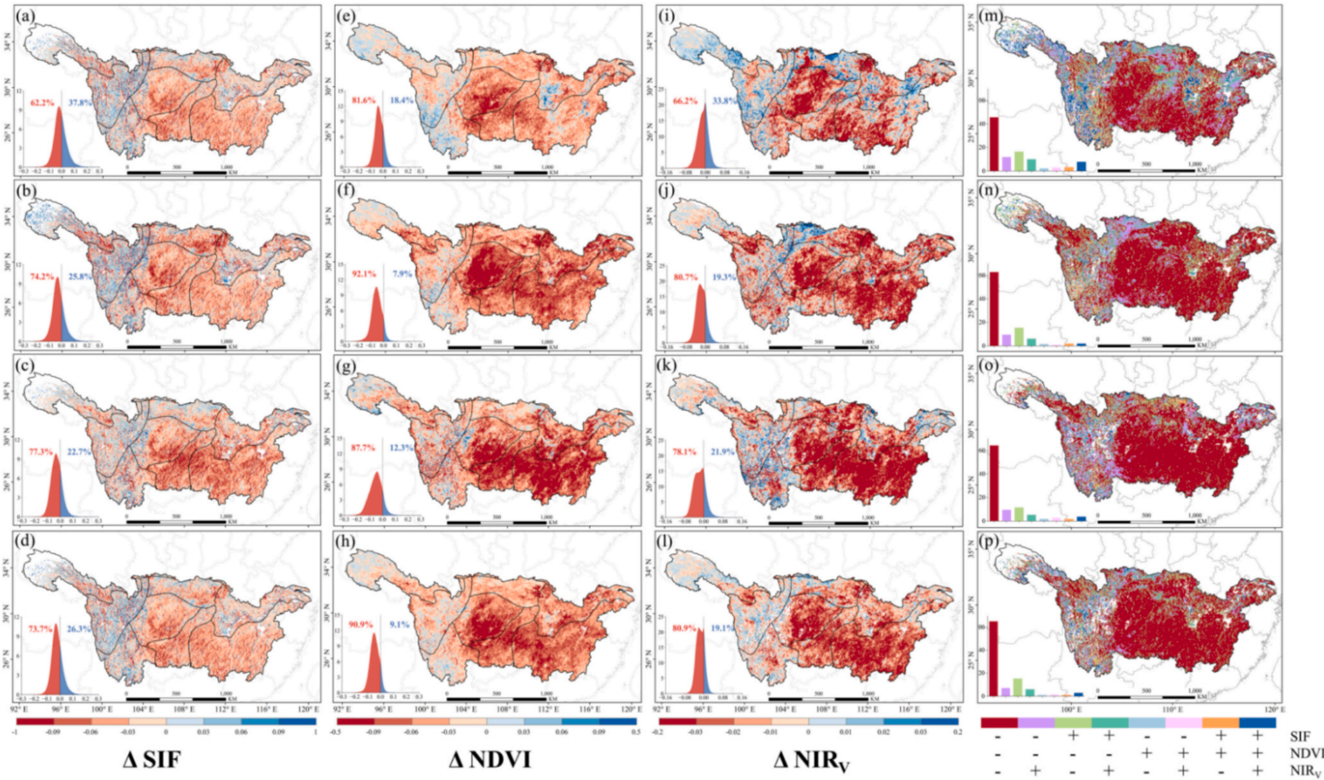

Fig. 5. Evolution processes and consistency of anomalies in SIF (ΔSIF: a–d), NDVI (ΔNDVI: e–h) and NIR_V (ΔNIR_V: i–l) in the Yangtze River basin during July, August, September and Summer of 2022. The values represent the percentage of pixels with positive and negative anomalies in vegetation indices, relative to the total number of pixels in the basin. The graph in the fourth column on the right side (m–p) depicts the spatial uniformity across three vegetation indices, while the small inset shows the proportion of pixels affected by the variations in detrended anomalies for these indices.

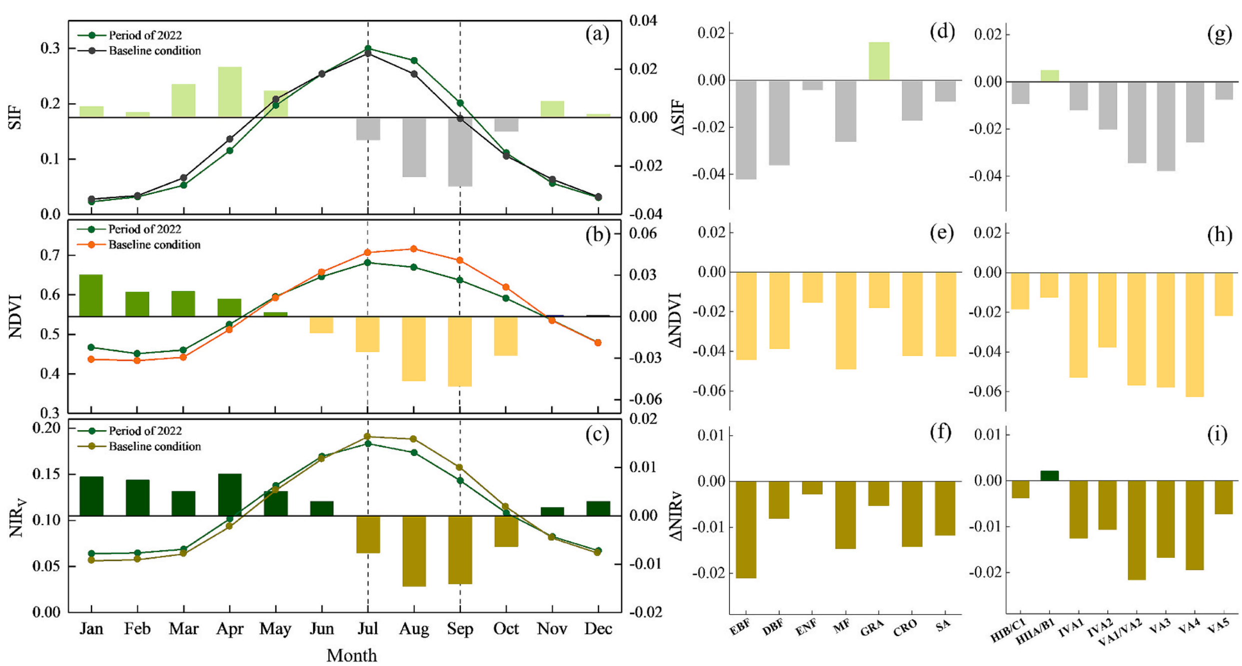

Fig. 6. Temporal variations of SIF (a), NDVI (b), and NIR_V (c) as well as the monthly anomalies relative to the baseline in the 2022 summer drought across the Yangtze River basin, China. The bar charts (d–f; g–i) represent the anomalies of the three vegetation indices (SIF, NDVI and NIR_V) in different vegetation types and eco-geographical zones in summer 2022, respectively.

SIF and NIR_V were faster than that of NDVI. During the early stages of the drought (June), the detrended SIF and NIR_V displayed a slight positive value, whereas NDVI showed a more pronounced negative anomaly (Fig. 6). By the end of the year (November), SIF and NIR_V had recovered to higher positive levels, while NDVI only reached a marginally positive state (Figs. S2–S4).

In the present study, the 2022 summer drought had varying impacts on the three vegetation indices across different vegetation types and eco-geographical zones. As a proxy for vegetation structural characteristics, NDVI was the most affected during this event, with significant negative anomalies detected across all the vegetation types (Fig. 6b). Forests, which cover 28 % of the YRB, showed heightened sensitive to the extreme drought in 2022 summer (Fig. 6d–f). Among the forest types, EBF and MF were most affected by such drought event, followed by DBF, with ENF being the least affected. In contrast, grasslands, mainly distributed in the high-altitude regions of YRB, were less affected by the summer of 2022 drought, which even showed a slight increase in SIF (Fig. 6d). Croplands and savannas experienced a similar magnitude of decline in response to the drought, as indicated by SIF, NDVI, and NIR_V (Fig. 6d–f). Additionally, the response of vegetation indices across eco-geographical zones demonstrated consistent patterns in SIF and NIR_V (Fig. 6g, i). Within the YRB, the regions at lower altitudes faced a more severe and extended period of drought conditions during the summer of 2022. Our results indicated that significant vegetation dynamics anomalies were mainly distributed in the subtropical regions, especially in the VA3, VA4 and VA1/VA2 (Fig. 6g–i and Figs. S2–S4). Additionally, the anomalies of the three vegetation indices in the VA3 and VA1/VA2 peaked in September whereas the VA4 peaked in July and August (Figs. S2–S4), suggesting that the resistance of vegetation dynamics to extreme drought varied over different eco-geographical zones.

3.3. Vegetation resistance and resilience to the 2022 summer drought

The average vegetation resistance and the duration of resistance throughout the summer drought of 2022 were evaluated across the YRB (Fig. 7a-b). Spatially, high-altitude regions generally exhibited stronger vegetation resistance, with values of about 0.83. By contrast, the Guizhou Plateau, Jiangnan Hills, and parts of the Sichuan Basin exhibited lower vegetation resistance. The Jiangnan Hills recorded the lowest vegetation resistance, with a value of only 0.54. Specifically, vegetation resistance across most areas ranged from 0.3 to 0.9, with the percentage of the pixels accounting for 51.7 % and 26.6 % of YRB, respectively. Our findings revealed that resistance time and resistance exhibited opposite patterns in certain regions, such as the VA3 and VA1/VA2, with the average resistance time lasting approximately three months. Notably, both the resistance and resistance time in the Sichuan Basin were relatively low. Furthermore, we compared the magnitude of vegetation resistance and resistance time across different biomes (Fig. 8). The average values of vegetation resistance were as follows: EBF (0.63), SA (0.65), ENF (0.68), MF (0.68), DBF (0.71) and GRA (0.86). Grasslands situated in high-altitude areas exhibited stronger vegetation resistance. In contrast, forests generally displayed lower vegetation resistance compared to other biomes, with EBF demonstrating the lowest levels of resistance.

A large portion of the areas showed a period of vegetation resilience that was roughly less than three months in duration, with shorter resistance times noted in the Sichuan Basin and the middle and lower reaches of the Yangtze River. In the YRB, vegetation in plain areas exhibited longer resistance times compared to mountainous regions, particularly in the Jiangnan Hills and the eastern part of the Guizhou Plateau. This implies that vegetation in these regions is more resilient to droughts. In contrast to vegetation resistance, the resistance time of various biomes showed an opposite trend. The majority of forest vegetation had a longer resistance time (2.56 months), while grasslands had a shorter resistance time (1.81 months). Among the various forest types, EBF exhibited the lowest resistance and the longest resistance time.

The average vegetation resilience and recovery time during 2022 summer drought were evaluated in the YRB (Fig. 7c-d). Specifically, vegetation resilience in most areas ranged from 2 to 4, accounting for 53.8 % and 25.9 %, respectively. Enhanced vegetation recovery was predominantly observed in the majority of areas within VA1/VA2, with resilience values peaking at 3, whereas diminished vegetation recovery was noted in the western segment of the YRB, particularly in the VA5 and HIB1/C1. The magnitude of vegetation recovery time was illustrated in Fig. 7d. In most regions, the vegetation recovery time following the drought ranged from 14 to 17 months. It is evident that the vegetation recovery time in hilly areas, such HIIA/B1 and HIB1/C1, was longer than in plain areas. On the other hand, more of regions in the IVA1 demonstrated shorter recovery times, averaging about 13 months.

The magnitude of vegetation resilience and recovery time across various biomes was accessed in Fig. 8. The resilience of forests and savannas was higher than that of croplands and grasslands. Remarkably, among all forest types, DBF exhibited the lowest resilience. Significant differences in vegetation recovery time were observed between

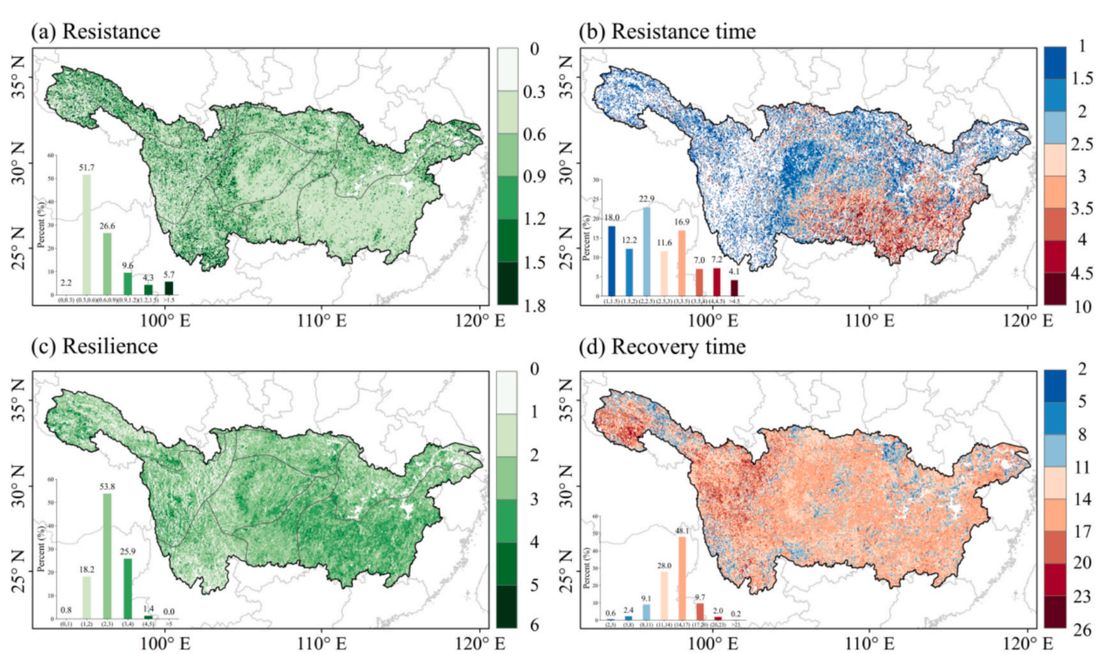

Fig. 7. Spatial patterns of vegetation resistance (a), resistance time (b), resilience (c) and recovery time (d) to summer drought of 2022, with the inset bar charts representing the percentage of the pixels varied different intervals.

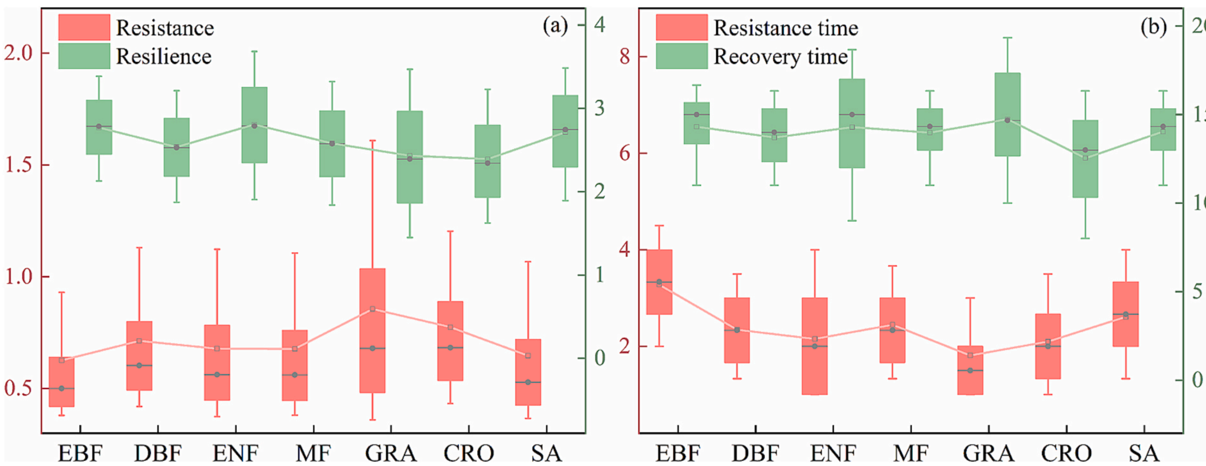

Fig. 8. Magnitudes of vegetation resistance, resilience (a), resistance time and recovery time (b) to summer drought of 2022 across different vegetation types. The box boundaries indicate the 25th–75th percentile. The whiskers extend from the box boundary to the largest and smallest values (1.5 × interquartile range). The solid line and dot inside the box show the median value.

croplands and other vegetation types. The following order of increases in average vegetation recovery time was observed: CRO (12.5), DBF (13.7), MF (14), SA (14), EBF (14.3), ENF (14.3) and GRA (14.7). The shorter recovery time in croplands can be attributed to agricultural irrigation practices.

In summary, our study reveals the spatio-temporal heterogeneity of vegetation resistance and resilience during the 2022 summer drought in the YRB and their associations with vegetation types. Spatially, high-altitude regions exhibited stronger vegetation resistance, while lowland ecosystems such as the Guizhou Plateau, Jiangnan Hills, and Sichuan Basin showed significantly lower resistance. Notably, a regional inverse relationship between vegetation resistance and resistance duration was observed. For instance, the Sichuan Basin exhibited both low resistance and short resistance duration, whereas forests, despite generally lower resistance, demonstrated longer resistance maintenance periods, highlighting their phased adaptive strategies to drought. In terms of resilience, forests and savannas exhibited superior recovery capacity compared to croplands and grasslands, albeit with significantly longer recovery times. In contrast, croplands recovered the fastest due to irrigation interventions, highlighting the regulatory role of human activities in ecological recovery. The interaction between geographic environment and vegetation type was pronounced: hilly areas generally had longer recovery times than plains, while vegetation in the Jiangnan Hills and eastern Guizhou Plateau displayed larger post-drought recovery potentials.

3.4. Vegetation vulnerability to the 2022 summer drought

We further explored the relationship between indicators of vegetation resistance and resilience. Here, we calculated the spatial distribution of vulnerability in the YRB and assessed its magnitude of vulnerability across different vegetation types (Fig. 9). Specifically, vegetation vulnerability in most areas ranged from 0.4 to 0.8, with the percentage of the pixels accounting for 25.4 % and 43.4 % of YRB, respectively. High vegetation vulnerability values were particularly noted in the southeastern part of the YRB, especially in the Jiangnan Hills (0.72), while lower vulnerability values were observed in the high-altitude regions of the western YRB. In order to investigate the extent of vegetation vulnerability across various biomes, boxplots of vegetation vulnerability were shown in Fig. 9. Stronger average vegetation vulnerability in EBF (0.69) and MF (0.68) were revealed, followed by SA (0.67), DBF (0.64), CRO (0.64), ENF (0.62) and GRA (0.61). Among the various biomes, forests displayed the highest vulnerability. Consequently, vegetation in the VA4 and VA1/VA2 was found to be more vulnerable compared to other regions. Notably, the vegetation vulnerability in the middle and lower YRB was relatively low, likely due to the high proportion of cropland benefiting from anthropogenic irrigation.

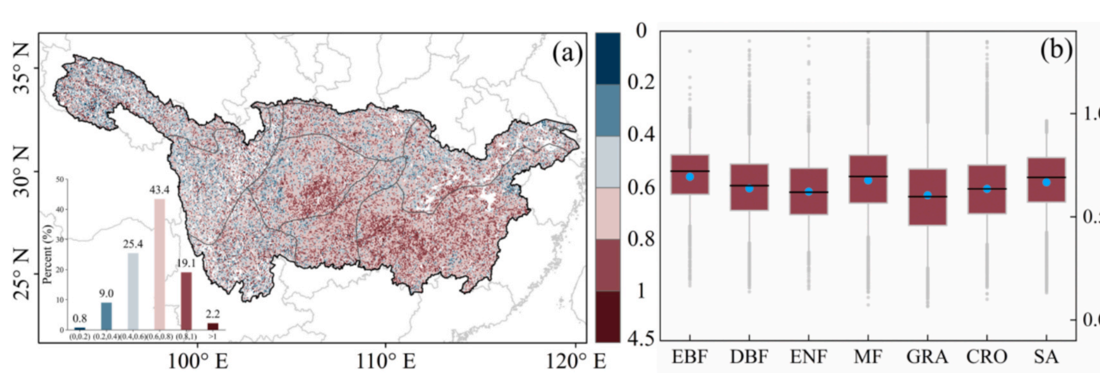

Fig. 9. Spatial patterns (a) of vegetation vulnerability to the summer drought event in 2022, with the boxplots (b) representing the magnitudes of vulnerability across different vegetation types. The box boundaries indicate the 25th–75th percentile. The whiskers extend from the box boundary to the largest and smallest values (1.5 × interquartile range). The solid line and blue dot inside the box show the median and mean value, respectively. The gray points are outliers. (For interpretation of the references to colour in this figure legend, the reader is referred to the web version of this article.)

4. Discussion

4.1. Drought-induced effects on vegetation dynamics

In the summer of 2022, the YRB experienced a typical compound event characterized by extreme high temperature and drought, notable for its intensity, duration, and extensive impact (Hao et al., 2023). According to a recent research, the extreme drought event that broke records was partly caused by anomalous anticyclone circulation in the mid-upper troposphere over northern, central, and eastern China (Wang et al., 2023b). Our findings indicated that the summer drought of 2022 ranks among the most severe events ever recorded in China, with a return period estimated at tens of thousands of years. In September, the entire YRB was in a state of drought (Fig. 4c). Furthermore, extreme drought events can pose significant threats to the stability of both society and ecosystems. For example, a recent study indicated that extreme drought event, such as forest wildfires, in summer of 2022 severely impacted the energy, food, water, and ecological sectors in the southwestern region (Xu et al., 2024). Our research provides an important and timely evaluation of the potential consequences of such event across the YRB.

The analysis reveals that the 2022 summer drought significantly suppressed vegetation status and, to some extent, disturbed the region carbon cycles. In general, this event resulted in the most severe declines in SIF by 0.02, the NDVI by 0.05 and the NIR_V by 0.02 since summer of 2003 (see Fig. 5). However, it is important to note that not all droughts lead to reduced productivity in biological communities (Li et al., 2023b; Xu et al., 2024). Our study found that high-altitude areas were less affected by this drought event compared to other regions, with a slight increase in SIF and NIR_V observed in the Western Sichuan-Eastern Tibet Plateau. This increase may reflect the physiological adaptation mechanism of vegetation under drought stress. For example, plants may experience increased non-photochemical quenching under water stress, leading to increased SIF, but this does not imply increased photosynthetic efficiency and may be an indicator of stress (Helm et al., 2020). In addition, high-altitude grassland ecosystems may have different water use strategies, such as deeper root systems or different phenological cycles, that allow them to maintain or increase photosynthesis during droughts (Wang, 2024). Moreover, existing studies have indicated that elevation is a key variable influencing vegetation growth, and the spatial distribution of elevation-related warming plays a significant role in driving vegetation greening patterns (Wang et al., 2021b). One of the most notable ecological responses to significant warming in high-altitude areas is the extension of the growing season, which allows for an increase in the greenness of vegetation previously limited by low temperatures (Wang et al., 2021b; Zou et al., 2020). In karst areas, the soil layer is shallow, and the water holding capacity is poor, as a result, much of the precipitation quickly flows into the underground karst system through pipes or fissures. This leads to a substantial reduction in available soil water, which explains the significant impact of the drought on the Sichuan Basin and Guizhou Plateau (Jiang et al., 2014; Long et al., 2014). In contrast, the middle and lower reaches of the Yangtze River, where cropland is the dominant vegetation type, effectively mitigated the negative impacts of the extreme drought through measures such as human-managed water conservation.

Vegetation growth in different ecosystem types responded differently to the drought. Overall, our findings indicated that forest ecosystems contributed the most to the negative anomalies observed in the three VIs (Fig. 5d–f), in line with previous studies (Wang et al., 2023a; Li et al., 2024). Among them, EBF exhibited the highest sensitivity to drought. Severe drought conditions led to changes in forest canopy structure, including leaf shedding and browning, which subsequently reduced photosynthesis rates and overall vegetation greenness (Jiang et al., 2022). Additionally, during prolonged drought, forests relied on water absorption from deep-rooted soils; this dependence can delay tree growth (Anderegg et al., 2015). Furthermore, our result supported the notion that croplands were highly susceptible to drought. In agricultural ecosystems, many crops usually have shorter root systems and depend mostly on surface soil moisture, which quickly evaporates during droughts without timely precipitation replenishment (Chen et al., 2024). In contrast, alpine coniferous forests and alpine grasslands benefited from the melting of ice and snow, which significantly mitigated the adverse effects of drought, consistent with previous findings (Gharun et al., 2020). In terms of forest types, the resilience of deciduous DBF is higher than that of EBF and ENF.

Contrary to some other studies (Xu et al., 2024; Wang et al., 2019; Song et al., 2018), our analysis indicated that NDVI reacted to drought events more quickly than SIF and NIR_V, especially when plants perceived a low water supply because of soil moisture deficiencies or high atmospheric water demand (Fig. 6). This discrepancy might be explained by several mechanisms. Firstly, physiological adaptations in plants often prioritize photosynthesis to sustain the energy required for growth and survival during drought conditions. Such adaptations can lead to a reduction in NDVI due to the negative effects of drought, while simultaneously improving photosynthetic efficiency, as evidenced by increased SIF and NIR_V (Chen et al., 2024). Secondly, plants may show signs of heat stress in reaction to high temperatures, such as modifications to photosynthesis and defense of other physiological functions. Furthermore, our study showed that SIF and NIR_V, as physiological proxies of vegetation, showed outstanding consistency in drought monitoring. Due to their benefits in directly assessing plant photosynthetic processes, these two VIs have been used for drought evaluations (Ding et al., 2022; Li et al., 2024; Wang et al., 2023a).

4.2. Vegetation feedbacks to drought extremes

Drought presented a significant challenge to the stability of ecosystem structure and function. Grasp of vegetation's capacity to resist and recover is crucial for monitoring vegetation changes in the YRB, especially with the heightened probability and recurrence of severe droughts. Previous studies have reported a trade-off between drought resistance and resilience in ecosystems at different spatial scales, identified as a pattern of strong resistance with weak resilience or weak resistance with strong resilience (Yao et al., 2024; Sturm et al., 2022), which is generally consistent with our findings. However, forests in the Sichuan Basin and Guizhou Plateau exhibited low vegetation resistance and resilience. These regions are predominantly characterized by karst landscapes, where the thin soil layer has a low water retention capacity. As a result, water use efficiency in the karst regions is significantly lower in comparison with the non-karst regions, impairing their capacity to adapt to extreme drought events (Liu et al., 2023b; Helman et al., 2017; Li et al., 2019). In our study, these regions experienced higher drought exposure compared to high-altitude areas, compounded by groundwater scarcity and widespread wildfire outbreaks, collectively indicating a lower resistance capacity of forest ecosystems to this event. In contrast, alpine meadows in the Qinghai-Tibet Plateau demonstrated high vegetation resistance, align with previous studies (Wang et al., 2022; Wang et al., 2020). A potential explanation for this finding was the high biodiversity present in the alpine meadow, which could enhance the vegetation's resistance to this summer drought event (Huang et al., 2021b). Additionally, croplands in the Middle and Lower Yangtze River basin were greatly affected by the human activities. Irrigation and effective farmland management practices provided the necessary water resources in short time spans, thereby enhancing vegetation resistance in the irrigated croplands (Huang et al., 2021a; Jiang et al., 2024).

Vegetation resilience in the YRB was found to follow a distinct pattern than vegetation resistance. In line with earlier study (Huang et al., 2021b), the alpine steppe and meadow ecosystems on the Qinghai-Tibet Plateau exhibited the strongest resistance but the lowest resilience, accompanied by the longest recovery times. Insufficient rainfall led to excessive consumption of soil moisture during the drought year, resulting in depleted soil moisture in the subsequent year. This, in turn, contributed to lower resilience and extended recovery times (Liu et al., 2021; Huang et al., 2021b). In contrast, forest ecosystems, by utilizing deeper root systems and more conservative water-use strategies, were able to recover quickly after the drought (Duan et al., 2019; Zhao et al., 2023; Qi et al., 2021). Our findings suggest that CRO has a higher resilience. CRO is a specific highly managed ecosystem rather than a natural one, and its resilience is largely related to human-induced management practices such as tillage and irrigation. This favorable condition for water availability might contribute to the higher resistance of GRA in these regions (Li et al., 2025).

By combining the vegetation resistance and resilience indices, we calculated the spatial distribution of vegetation vulnerability across the YRB and assessed the vulnerability levels of different vegetation types (Fig. 9). Alpine grasslands, controlled by climatic exposure, exhibit low vulnerability. This suggests that despite harsh environmental conditions, these ecosystems have adapted to withstand climate stressors, making them less susceptible to disturbances like droughts compared to other ecosystems (Li et al., 2020a). Larger vulnerability was observed in the EBF and MF of VA4 and VA1/VA2. Existing research has found a significant decline in global vegetation resistance, with EBF experiencing the largest decrease, which implies the increasing vulnerability of forest ecosystem to withstand future droughts (Huang and Xia, 2019; Liu et al., 2023a).

Post-drought recovery of vegetation productivity (e.g., NDVI, GPP) often lags due to hydraulic damage (Anderegg et al., 2015). Therefore, the drought legacy effects on vegetation recovery can not be neglected which are generally shaped by drought intensity, duration, ecosystem type, and post-drought environmental conditions (Schwalm et al., 2017; Liu et al., 2025). The extreme drought in 2022 led to significant depletion of soil moisture, especially in regions like the Sichuan Basin and Guizhou Plateau. This depletion persisted into subsequent years, affecting the recovery of vegetation structure and function. The recovery time for different vegetation types can vary significantly. For example, the study found that in karst regions, the thin soil layer and poor water retention capacity resulted in prolonged recovery times for vegetation, particularly for forests (Liu et al., 2021; Huang et al., 2021b). Croplands, due to human intervention such as irrigation, had the shortest recovery time (12.5 months). Furthermore, the recovery time usually increases with drought severity (Wang et al., 2025). For example, a 1-standard-deviation increase in drought intensity prolongs recovery by 3–6 months in temperate ecosystems, where as extreme droughts (e.g., $>3\sigma$ below mean precipitation) can delay recovery for 2–4 years in forests (Schwalm et al., 2017). Then, longer droughts amplify legacy effects (Yao et al., 2022). The recovery rates slow by ~10–20 % per additional month of drought in semi-arid regions (Xu et al., 2022). Thus, legacy effects complicate predictions of ecosystem resilience under climate change, while incorporating drought history and recovery thresholds into ecological process models is critical for carbon cycle projections and land management.

4.3. Limitations and implications

Our study comprehensively analyzed the impacts of the 2022 summer drought in the YRB on vegetation dynamics using three remote sensing-derived vegetation indices, and attempted to develop a novel resistance-resilience framework to quantitatively characterize vegetation stability at the ecosystem scale under intensified drought conditions, while exploring potential ecophysiological mechanisms underlying these responses. However, the accuracy of our findings fundamentally depend upon the precision of remote sensing products, with inherent uncertainties in sensor calibration, atmospheric correction, and spatiotemporal resolution requiring explicit consideration during ecological interpretation. Besides, our analysis of resistance and resilience of ecosystems focused on monthly scales, but critical ecosystem drought responses may operate at finer timescales (e.g., daily/weekly). Advancing remote sensing technology could enable higher-resolution temporal data to better resolve ecosystem drought response dynamics. Generally, the intrinsic ecophysiological trade-off between vegetation resistance and resilience remains unclear. We advocate for future multi-scale investigations synthesizing in flux-site observations, remote sensing data, and modeling approaches across organismal, regional, and global scales to elucidate the mechanistic basis of this critical vegetation adaptation strategy.

Our study reveals significant negative impacts of the 2022 summer drought on vegetation dynamics across the Yangtze River Basin, with pronounced spatial heterogeneity in drought responses among different ecogeographical zones. Forest ecosystems exhibited particularly high drought vulnerability, as evidenced by substantial negative anomalies in vegetation indices and reduced resistance capacity. Notably, EBFs demonstrated the highest ecosystem vulnerability, underscoring the urgent need for global conservation efforts targeting these critical ecosystems. Previous studies have established EBFs' pivotal role in sustaining global vegetation productivity under extreme drought conditions (Huang and Xia, 2019). More evidence demonstrates a strong correlation between vegetation drought resistance and functional traits, with mixed communities enhancing ecosystem stability (Isbell et al., 2015). Consequently, we recommend implementing gradient-based ecological management strategies in future forest conservation practices: prioritizing natural regeneration in high-resilience zones while applying assisted restoration in low-resilience areas, coupled with functional trait-oriented mixed-species forestation initiatives.

5. Conclusions

Our study presented the characteristics and evolution trends of the 2022 summer drought in the Yangtze River basin, China. By utilizing three satellite-derived vegetation indices, we investigated the effect of extreme drought event on vegetation growth and quantitatively analyzed the resistance, resilience and vulnerability of vegetation to such event. Our findings are concluded as follows:

(1) The YRB experienced its most extreme summer drought since 2003 in 2022, characterized by an average temperature increase of 1 °C and a precipitation deficit of 206.3 mm. The drought significantly reduced critical vegetation indices, with decreases of 0.01 in SIF, 0.02 in NDVI, and 0.01 in NIR_V, respectively. Moreover, the Sichuan Basin, Hanzhong Basin, and middle-lower reaches of the Yangtze River were most severely impacted, while high-altitude regions exhibited relatively milder effects.

(2) During the summer of 2022, the YRB exhibited widespread negative detrended anomalies in vegetation indices, with 73.7 % of GOSIF, 90.9 % of NDVI, and 80.9 % of NIR_V indicating significant declines in photosynthetic activity. Ecogeographically, negative anomalies were concentrated in lowland regions such as the Sichuan Basin, Guizhou Plateau, and Jiangnan Hills, contrasting with positive anomalies observed in high-altitude areas like the Tibetan Plateau, Western Sichuan Valleys, and Yunnan Plateau. Vegetation responses varied markedly by biome: forest ecosystems, particularly evergreen broadleaf and mixed forests, were most sensitive to drought stress, showing the largest reductions in indices, followed by deciduous broadleaf and coniferous forests. In contrast, croplands experienced only marginal declines due to anthropogenic irrigation, while grasslands demonstrated minimal impacts.

(3) Ecogeographical analysis revealed distinct patterns in vegetation resistance and resilience across the YRB. High-altitude regions exhibited strong vegetation resistance but short resistance duration, whereas the Guizhou Plateau and Jiangnan Hills showed low resistance but prolonged resistance periods. The Sichuan Basin was notably vulnerable, with both low resistance and short resistance duration. In terms of resilience, the Jiangnan Hills

displayed high recovery capacity, contrasting with low resilience in western regions such as the Yunnan Plateau and Tibetan Plateau. Vegetation recovery time in high-altitude areas exceeded that of plains. Biome-specific responses further highlighted these dynamics: alpine meadows and croplands demonstrated strong resistance, while forests—particularly evergreen broadleaf forests—had the lowest resistance. Forests and savannas outperformed croplands and grasslands in resilience. Notably, evergreen broadleaf and mixed forests in karst-affected areas (e.g., the Sichuan Basin and Guizhou Plateau) were highly vulnerable, facing escalating risks from extreme droughts under global warming.

Overall, the trade-off between vegetation resistance and resilience provides critical insights for adaptive ecosystem management. These findings underscore the need to optimize biome composition and water resource allocation based on regional ecological baselines, thereby enhancing compound ecological resilience under drought threat.

CRediT authorship contribution statement

Lei Han: Writing – original draft, Formal analysis. **Yanan Chen:** Data curation. **Chaoyang Wu:** Writing – review & editing. **Li Yao:** Writing – review & editing, Funding acquisition. **Ying Wang:** Methodology. **Chao Su:** Software, Resources. **Xuan Li:** Visualization. **Alexandre Maniçoba da Rosa Ferraz Jardim:** Writing – review & editing. **Thieres George Freire da Silva:** Writing – review & editing. **Xuguang Tang:** Writing – review & editing, Conceptualization.

Declaration of competing interest

The authors declare the following financial interests/personal relationships which may be considered as potential competing interests: Li Yao reports financial support was provided by National Natural Science Foundation of China. If there are other authors, they declare that they have no known competing financial interests or personal relationships that could have appeared to influence the work reported in this paper.

Acknowledgments

This study was jointly supported by the National Natural Science Foundation of China (Grant No. 41901145) and the Graduate Scientific Research and Innovation Foundation of Southwest University (Grant No. SWUS24095).

Appendix A. Supplementary data

Supplementary data to this article can be found online at https://doi.org/10.1016/j.jhydrol.2025.133673.

Data availability

Data will be made available on request.

References

AghaKouchak, A., Chiang, F., Huning, L.S., Love, C.A., Mallakpour, I., Mazdiyasni, O., Sadegh, M., 2020. Climate extremes and compound hazards in a warming world. Annu. Rev. Earth Planet. Sci. 48, 519–548.
Anderegg, W.R., Schwalm, C., Biondi, F., Camarero, J.J., Koch, G., Litvak, M., Pacala, S., 2015. Pervasive drought legacies in forest ecosystems and their implications for carbon cycle models. Science 349 (6247), 528–532.
Badgley, G., Field, C.B., Berry, J.A., 2017. Canopy near-infrared reflectance and terrestrial photosynthesis. Sci. Adv. 3 (3), e1602244.
Bai, P., Liu, X., Zhang, Y., Liu, C., 2020. Assessing the impacts of vegetation greenness change on evapotranspiration and water yield in China. Water Resour. Res. 56 (10), e2019WR027019.
Bellanthudawa, B.K.A., Chang, N.B., 2022. Spectral index-based time series analysis of canopy resistance and resilience in a watershed under intermittent weather changes. Eco. Inform. 69, 101666.
Chen, C., He, B., Guo, L., Zhang, Y., Xie, X., Chen, Z., 2018. Identifying critical climate periods for vegetation growth in the Northern Hemisphere. J. Geophys. Res. Biogeosci. 123 (8), 2541–2552.
Chen, J., Jönsson, P., Tamura, M., Gu, Z., Matsushita, B., Eklundh, L., 2004. A simple method for reconstructing a high-quality NDVI time-series data set based on the Savitzky–Golay filter. Remote Sens. Environ. 91 (3–4), 332–344.
Chen, S., Qiu, R., Chen, Y., Gong, W., Han, G., 2024. Impacts of drought and heatwave on the vegetation and ecosystem in the Yangtze River basin in 2022. Remote Sens. (Basel) 16 (16), 2889.
Chen, X., Wang, L., Niu, Z., Zhang, M., Li, J., 2020. The effects of projected climate change and extreme climate on maize and rice in the Yangtze River Basin, China. Agric. For. Meteorol. 282, 107867.
Chen, Y., Wang, Y., Wu, C., et al., 2025. Drought-induced stress on rainfed and irrigated agriculture: insights from multi-source satellite-derived ecological indicators. Agric. Water Manag. 307, 109249.
Ciais, P., Reichstein, M., Viovy, N., Granier, A., Ogée, J., Allard, V., Valentini, R., 2005. Europe-wide reduction in primary productivity caused by the heat and drought in 2003. Nature 437 (7058), 529–533.
Cole, L.E., Bhagwat, S.A., Willis, K.J., 2014. Recovery and resilience of tropical forests after disturbance. Nat. Commun. 5 (1), 3906.
De Keersmaecker, W., Lhermitte, S., Honnay, O., Farifteh, J., Somers, B., Coppin, P., 2014. How to measure ecosystem stability? An evaluation of the reliability of stability metrics based on remote sensing time series across the major global ecosystems. Glob. Chang. Biol. 20 (7), 2149–2161.
De Keersmaecker, W., Lhermitte, S., Tits, L., Honnay, O., Somers, B., Coppin, P., 2015. A model quantifying global vegetation resistance and resilience to short-term climate anomalies and their relationship with vegetation cover. Glob. Ecol. Biogeogr. 24 (5), 539–548.
Ding, Y., Xu, J., Wang, X., Peng, X., Cai, H., 2020. Spatial and temporal effects of drought on Chinese vegetation under different coverage levels. Sci. Total Environ. 716, 137166.
Ding, Y., He, X., Zhou, Z., Hu, J., Cai, H., Wang, X., Shi, H., 2022. Response of vegetation to drought and yield monitoring based on NDVI and SIF. Catena 219, 106328.
Duan, H., Li, Y., Xu, Y., Zhou, S., Liu, J., Tissue, D.T., Liu, J., 2019. Contrasting drought sensitivity and post-drought resilience among three co-occurring tree species in subtropical China. Agric. For. Meteorol. 272, 55–68.
García-Herrera, R., Díaz, J., Trigo, R.M., Luterbacher, J., Fischer, E.M., 2010. A review of the European summer heat wave of 2003. Crit. Rev. Environ. Sci. Technol. 40 (4), 267–306.
Gazol, A., Camarero, J.J., Vicente-Serrano, S.M., Sánchez-Salguero, R., Gutiérrez, E., de Luis, M., Galván, J.D., 2018. Forest resilience to drought varies across biomes. Glob. Chang. Biol. 24 (5), 2143–2158.
Gharun, M., Hörtnagl, L., Paul-Limoges, E., Ghiasi, S., Feigenwinter, I., Burri, S., Buchmann, N., 2020. Physiological response of swiss ecosystems to 2018 drought across plant types and elevation. Philos. Trans. R. Soc. B 375 (1810), 20190521.
Han, L., Chen, Y., Wang, Y., Sun, Y., Ding, Z., Zhang, H., Tang, X., 2024. Divergent responses of subtropical evergreen and deciduous forest carbon cycles to the summer 2022 drought. Environ. Res. Lett. 19 (5), 054043.
Hao, Z., Zhang, X., Hao, F., et al., 2023. Impacts and coping strategies of compound hot extremes and droughts during summer of 2022 in the Yangtze River Basin. Water Resour. Prot. 39 (6), 46–52.
Helm, L.T., Shi, H., Lerdau, M.T., Yang, X., 2020. Solar-induced chlorophyll fluorescence and short-term photosynthetic response to drought. Ecol. Appl. 30 (5), e02101.
Helman, D., Osem, Y., Yakir, D., Lensky, I.M., 2017. Relationships between climate, topography, water use and productivity in two key Mediterranean forest types with different water-use strategies. Agric. For. Meteorol. 232, 319–330.
Huang, W., Wang, W., Cao, M., Fu, G., Xia, J., Wang, Z., Li, J., 2021a. Local climate and biodiversity affect the stability of China's grasslands in response to drought. Sci. Total Environ. 768, 145482.
Huang, L., Zhou, P., Cheng, L., Liu, Z., 2021b. Dynamic drought recovery patterns over the Yangtze River Basin. Catena 201, 105194.
Huang, S., Gan, Y., Zhang, X., Chen, N., Wang, C., Gu, X., Niyogi, D., 2023. Urbanization amplified asymmetrical changes of rainfall and exacerbated drought: Analysis over five urban agglomerations in the Yangtze River Basin, China. Earth's Future 11 (2), e2022EF003117.
Huang, S., Tang, L., Hupy, J.P., Wang, Y., Shao, G., 2021c. A commentary review on the use of normalized difference vegetation index (NDVI) in the era of popular remote sensing. J. For. Res. 32 (1), 1–6.
Huang, K., Xia, J., 2019. High ecosystem stability of evergreen broadleaf forests under severe droughts. Glob. Chang. Biol. 25 (10), 3494–3503.
Ingrisch, J., Bahn, M., 2018. Towards a comparable quantification of resilience. Trends Ecol. Evol. 33 (4), 251–259.
Isbell, F., Craven, D., Connolly, J., Loreau, M., Schmid, B., Beierkuhnlein, C., Eisenhauer, N., 2015. Biodiversity increases the resistance of ecosystem productivity to climate extremes. Nature 526 (7574), 574–577.
Jiang, L., Liu, B., Guo, H., Yuan, Y., Liu, W., Jiapaer, G., 2024. Assessing vegetation resilience and vulnerability to drought events in Central Asia. J. Hydrol. 634, 131012.
Jiang, Z., Lian, Y., Qin, X., 2014. Rocky desertification in Southwest China: Impacts, causes, and restoration. Earth Sci. Rev. 132, 1–12.
Jiang, W., Niu, Z., Wang, L., Yao, R., Gui, X., Xiang, F., Ji, Y., 2022. Impacts of drought and climatic factors on vegetation dynamics in the Yellow River Basin and Yangtze River Basin, China. Remote Sensing 14 (4), 930.

Li, D., Wu, S., Liu, L., Zhang, Y., Li, S., 2018. Vulnerability of the global terrestrial ecosystems to climate change. Glob. Chang. Biol. 24 (9), 4095–4106.

Li, G., Wu, C., Chen, Y., Huang, C., Zhao, Y., Wang, Y., Tang, X., 2023a. Increasing temperature regulates the advance of peak photosynthesis timing in the boreal ecosystem. Sci. Total Environ. 882, 163587.

Li, M., Zhang, X., He, Y., Niu, B., Wu, J., 2020a. Assessment of the vulnerability of alpine grasslands on the Qinghai-Tibetan Plateau. PeerJ 8, e8513.

Li, T., Wang, S., Chen, B., Wang, Y., Chen, S., Chen, J., Gu, P., 2024. Widespread reduction in gross primary productivity caused by the compound heat and drought in Yangtze River Basin in 2022. Environ. Res. Lett. 19 (3), 034048.

Li, X., Xiao, J., 2019. A global, 0.05-degree product of solar-induced chlorophyll fluorescence derived from OCO-2, MODIS, and reanalysis data. Remote Sens. (Basel) 11, 517.

Li, X., Piao, S., Wang, K., Wang, X., Wang, T., Ciais, P., Peñuelas, J., 2020b. Temporal trade-off between gymnosperm resistance and resilience increases forest sensitivity to extreme drought. Nat. Ecol. Evol. 4 (8), 1075–1083.

Li, X., Piao, S., Huntingford, C., Peñuelas, J., Yang, H., Xu, H., Mahecha, M.D., 2023b. Global variations in critical drought thresholds that impact vegetation. Natl. Sci. Rev. 10 (5), nwad049.

Li, X., Li, Y., Chen, A., Gao, M., Slette, I.J., Piao, S., 2019. The impact of the 2009/2010 drought on vegetation growth and terrestrial carbon balance in Southwest China. Agric. For. Meteorol. 269, 239–248.

Liu, Y., Zhang, Y., Peñuelas, J., Kannenberg, S.A., Gong, H., Yuan, W., Piao, S., 2025. Drought legacies delay spring green-up in northern ecosystems. Nat. Clim. Chang. 15, 444–451.

Li, Y., Zhuang, Q., Zhao, H., Zhang, W., Cai, P., Zhang, Y., Lv, J., 2025. Evaluation of the resistance and resilience of terrestrial ecosystems to drought in southwest China. J. Hydrol. 646, 132318.

Liu, Y., You, C., Zhang, Y., Chen, S., Zhang, Z., Li, J., Wu, Y., 2021. Resistance and resilience of grasslands to drought detected by SIF in inner Mongolia, China. Agric. For. Meteorol. 308, 108567.

Liu, Z., Zhu, J., Xia, J., Huang, K., 2023a. Declining resistance of vegetation productivity to droughts across global biomes. Agric. For. Meteorol. 340, 109602.

Liu, Y., Ding, Z., Chen, Y., Yan, F., Yu, P., Man, W., Tang, X., 2023b. Restored vegetation is more resistant to extreme drought events than natural vegetation in Southwest China. Sci. Total Environ. 866, 161250.

Long, D., Shen, Y., Sun, A., Hong, Y., Longuevergne, L., Yang, Y., Chen, L., 2014. Drought and flood monitoring for a large karst plateau in Southwest China using extended GRACE data. Remote Sens. Environ. 155, 145–160.

Meng, F., Huang, L., Chen, A., Zhang, Y., Piao, S., 2021. Spring and autumn phenology across the Tibetan Plateau inferred from normalized difference vegetation index and solar-induced chlorophyll fluorescence. Big Earth Data 5 (2), 182–200.

Mitchell, P.J., O'Grady, A.P., Pinkard, E.A., Brodribb, T.J., Arndt, S.K., Blackman, C.J., Tissue, D.T., 2016. An ecoclimatic framework for evaluating the resilience of vegetation to water deficit. Glob. Chang. Biol. 22 (5), 1677–1689.

Muñoz-Sabater, J., Dutra, E., Agustí-Panareda, A., Albergel, C., Arduini, G., Balsamo, G., Thépaut, J.N., 2021. ERA5-land: a state-of-the-art global reanalysis dataset for land applications. Earth Syst. Sci. Data 13 (9), 4349–4383.

Naresh Kumar, M., Murthy, C.S., Sesha Sai, M.V.R., Roy, P.S., 2009. On the use of Standardized Precipitation Index (SPI) for drought intensity assessment. Meteorol. Appl. 16 (3), 381–389.

Nimmo, D.G., Mac Nally, R., Cunningham, S.C., Haslem, A., Bennett, A.F., 2015. Vive la résistance: reviving resistance for 21st century conservation. Trends Ecol. Evol. 30 (9), 516–523.

Pettorelli, N., Vik, J.O., Mysterud, A., Gaillard, J.M., Tucker, C.J., Stenseth, N.C., 2005. Using the satellite-derived NDVI to assess ecological responses to environmental change. Trends Ecol. Evol. 20 (9), 503–510.

Piao, S., Zhang, X., Chen, A., Liu, Q., Lian, X., Wang, X., Wu, X., 2019. The impacts of climate extremes on the terrestrial carbon cycle: a review. Sci. China Earth Sci. 62, 1551–1563.

Qi, J.H., Fan, Z.X., Fu, P.L., Zhang, Y.J., Sterck, F., 2021. Differential determinants of growth rates in subtropical evergreen and deciduous juvenile trees: carbon gain, hydraulics and nutrient-use efficiencies. Tree Physiol. 41 (1), 12–23.

Qiu, R., Li, X., Han, G., Xiao, J., Ma, X., Gong, W., 2022. Monitoring drought impacts on crop productivity of the US Midwest with solar-induced fluorescence: GOSIF outperforms GOME-2 SIF and MODIS NDVI, EVI, and NIRv. Agric. For. Meteorol. 323, 109038.

Schwalm, C.R., Anderegg, W.R., Michalak, A.M., Fisher, J.B., Biondi, F., Koch, G., Tian, H., 2017. Global patterns of drought recovery. Nature 548 (7666), 202–205.

Smith, A.M., Kolden, C.A., Tinkham, W.T., Talhelm, A.F., Marshall, J.D., Hudak, A.T., Gosz, J.R., 2014. Remote sensing the vulnerability of vegetation in natural terrestrial ecosystems. Remote Sens. Environ. 154, 322–337.

Song, L., Guanter, L., Guan, K., You, L., Huete, A., Ju, W., Zhang, Y., 2018. Satellite sun-induced chlorophyll fluorescence detects early response of winter wheat to heat stress in the Indian Indo-Gangetic Plains. Glob. Chang. Biol. 24 (9), 4023–4037.

Sturm, J., Santos, M.J., Schmid, B., Damm, A., 2022. Satellite data reveal differential responses of Swiss forests to unprecedented 2018 drought. Glob. Chang. Biol. 28 (9), 2956–2978.

Tang, X., Li, H., Ma, M., Yao, L., Peichl, M., Arain, A., Goulden, M., 2017. How do disturbances and climate effects on carbon and water fluxes differ between multi-aged and even-aged coniferous forests? Sci. Total Environ. 599, 1583–1597.

Thornthwaite, C.W., 1948. An approach toward a rational classification of climate. Geogr. Rev. 38 (1), 55–94.

Vicente-Serrano, S.M., Beguería, S., López-Moreno, J.I., 2010. A multiscalar drought index sensitive to global warming: the standardized precipitation evapotranspiration index. J. Clim. 23 (7), 1696–1718.

Wang, C., Chen, J., Lee, S.C., Xiong, L., Su, T., Lin, Q., Xu, C.Y., 2025. Response and recovery times of vegetation productivity under drought stress: Dominant factors and relationships. J. Hydrol. 655, 132945.

Wang, L., 2024. Impacts of multiple temporal and spatial scale drought on grassland vegetation dynamics in the Tibetan Plateau region of China, 1982–2015. Environ. Dev. 51, 101033.

Wang, M., Ding, Z., Wu, C., Song, L., Ma, M., Yu, P., Tang, X., 2021a. Divergent responses of ecosystem water-use efficiency to extreme seasonal droughts in Southwest China. Sci. Total Environ. 760, 143427.

Wang, J., Yan, R., Wu, G., Liu, Y., Wang, M., Zeng, N., Chen, J.M., 2023a. Unprecedented decline in photosynthesis caused by summer 2022 record-breaking compound drought-heatwave over Yangtze River Basin. Sci. Bull. 68 (19), 2160–2163.

Wang, S., Guo, L., He, B., Li, T., 2020. The stability of Qinghai-Tibet Plateau ecosystem to climate change. Phys. Chem. Earth Parts A/B/C 115, 102827.

Wang, X., Qiu, B., Li, W., Zhang, Q., 2019. Impacts of drought and heatwave on the terrestrial ecosystem in China as revealed by satellite solar-induced chlorophyll fluorescence. Sci. Total Environ. 693, 133627.

Wang, Y., Fu, B., Liu, Y., Li, Y., Feng, X., Wang, S., 2021b. Response of vegetation to drought in the Tibetan Plateau: elevation differentiation and the dominant factors. Agric. For. Meteorol. 306, 108468.

Wang, Y., Lv, W., Xue, K., Wang, S., Zhang, L., Hu, R., Niu, H., 2022. Grassland changes and adaptive management on the Qinghai–Tibetan Plateau. Nat. Rev. Earth Environ. 3 (10), 668–683.

Wang, Z., Luo, H., Yang, S., 2023b. Different mechanisms for the extremely hot central-eastern China in July–August 2022 from a Eurasian large-scale circulation perspective. Environ. Res. Lett. 18 (2), 024023.

Xing, L., Zhao, R., Sun, H., Li, M., Tan, Z., 2024. Analysis of drought characteristics and comparison of historical typical years with 2022 drought in the Yangtze River Basin. Nat. Hazards 120 (4), 3699–3718.

Xu, K., Yang, D., Yang, H., Li, Z., Qin, Y., Shen, Y., 2015. Spatio-temporal variation of drought in China during 1961–2012: a climatic perspective. J. Hydrol. 526, 253–264.

Xu, W., Yuan, W., Wu, D., Zhang, Y., Shen, R., Xia, X., Ciais, P., Liu, J., 2024. Impacts of record-breaking compound heatwave and drought events in 2022 China on vegetation growth. Agric. For. Meteorol. 344 (2024), 109799.

Xu, Y., Zhang, X., Hao, Z., Hao, F., Li, C., 2022. Systematic assessment of the development and recovery characteristics of hydrological drought in a semi-arid area. Sci. Total Environ. 836, 155472.

Yao, Y., Fu, B., Liu, Y., Li, Y., Wang, S., Zhan, T., Gao, D., 2022. Evaluation of ecosystem resilience to drought based on drought intensity and recovery time. Agric. For. Meteorol. 314, 108809.

Yao, Y., Liu, Y., Song, J., Tao, S., Li, Y., Wu, T., Fu, B., 2024. Declining tradeoff between resistance and resilience of ecosystems to drought. Earth's Future 12 (5), e2024EF004665.

Zeng, Y., Hao, D., Huete, A., Dechant, B., Berry, J., Chen, J.M., Chen, M., 2022. Optical vegetation indices for monitoring terrestrial ecosystems globally. Nat. Rev. Earth Environ. 3 (7), 477–493.

Zhang, J., Xiao, J., Tong, X., Zhang, J., Meng, P., Li, J., Yu, P., 2022. NIRv and SIF better estimate phenology than NDVI and EVI: Effects of spring and autumn phenology on ecosystem production of planted forests. Agric. For. Meteorol. 315, 108819.

Zhao, D., Zhang, Z., Zhang, Y., 2023. Soil moisture dominates the forest productivity decline during the 2022 China compound drought-heatwave event. Geophys. Res. Lett. 50 (17), e2023GL104539.

Zou, F., Li, H., Hu, Q., 2020. Responses of vegetation greening and land surface temperature variations to global warming on the Qinghai-Tibetan Plateau, 2001–2016. Ecol. Ind. 119, 106867.

Huete, A., Didan, K., Van Leeuwen, W., Miura, T., Glenn, E., 2010. MODIS vegetation indices. In: New York, N.Y. (Ed.), Land remote sensing and global environmental change: NASA's earth observing system and the science of ASTER and MODIS. Springer, New, York, pp. 579–602.